

Acoustic Directionality of Explosions as Scale-Model Volcanoes

Sarah Anne Ostergaard

A capstone report submitted to the faculty of

Brigham Young University

In partial fulfillment of the requirements for the degree of

Bachelor of Science

Tracianne B. Neilsen, Advisor

Department of Physics and Astronomy

Brigham Young University

December 17, 2020

Copyright © 2020 Ostergaard

All Rights Reserved



## ABSTRACT

### Acoustic Directionality of Explosions as Scale-Model Volcanoes

Sarah Anne Ostergaard

Department of Physics and Astronomy

Bachelor of Science

Since volcanic ash ejection can be hazardous, it is important not only to detect volcanic eruptions, but also determine what areas will be most affected. In order to better understand the directionality of sound propagation from volcanos, tests were conducted using explosions as scale-model volcanos. The goal of this research is to estimate the directionality of explosions from measurements on an arc not concentric with the origin of the explosion. A test was conducted in a grass-covered field using oxy-acetylene filled balloons that produced acoustic shock waves. The gas-filled balloons were placed in the ground in four hand-made “craters” of different shapes to produce different directionalities. Measurements were taken using both circular microphone arrays centered on each of the four crater locations and a single semi-circle array that was not concentric with any of the craters. By connecting the two measurements using a spherical spreading approximation for propagated sound, more is understood about the directionality on the semicircle setup. This study was done in preparation for a volcano hazards workshop with buried explosives.

Keywords: acoustic, acoustics, volcano, volcanoes, explosions, explosives, oxy-acetylene balloons, directivity, directionality, nonlinear acoustics, crater shape, scale-model volcano, nonconcentric, concentric

# Acknowledgments

---

I'd like to thank my advisor Dr. Tracianne Neilsen of the BYU Department of Physics and Astronomy. She was always willing to answer any questions I had whether research related or about life in general. She was a great mentor, and I learned a lot by working with her.

I'd also like to thank the members of my research team: Carla Wallace, Christian Lopez, Julio Escobedo, Margaret Grace Smith, Eric Lysenko, and Menley Hawkes. They were wonderful to work with and I enjoyed the friendships and community we formed.

Lastly, I'd like to thank the National Science Foundation and Brigham Young University Department of Physical and Mathematical Sciences for funding this project. I am so grateful for the experience that I gained that was made possible through the funding I received.

# Table of Contents

---

<b>Table of Contents .....</b>	<b>v</b>
<b>List of Figures .....</b>	<b>vii</b>
<b>List of Tables.....</b>	<b>viii</b>
<b>Chapter 1 Introduction.....</b>	<b>9</b>
1.1 Motivation .....	9
1.2 Background.....	9
1.2.1 <i>Volcano Acoustics</i> .....	9
1.2.2 <i>Explosions as Scale-Model Volcanoes</i> .....	11
1.3 Prior Work.....	12
1.4 Overview.....	14
<b>Chapter 2 Methods .....</b>	<b>15</b>
2.1 Buried Explosives Test .....	15
2.1.1 <i>Summary</i> .....	15
2.1.2 <i>Semicircle Microphone Array</i> .....	16
2.2 Oxy-Acetylene Balloons Test .....	17
2.2.1 <i>Summary</i> .....	17
2.2.2 <i>Circular Microphone Arrays</i> .....	19
2.3 Spherical vs. Nonlinear Propagation .....	20
2.4 Effective Flow Resistivity .....	23
<b>Chapter 3 Analysis and Results .....</b>	<b>26</b>

3.1	Oxy-Acetylene Balloons Analysis .....	26
3.1.1	<i>Preliminary Directionality Analysis</i> .....	26
3.1.2	<i>Identifying Peaks in Waveforms</i> .....	27
3.1.3	<i>Circle and Semicircle Comparisons</i> .....	29
3.2	Conclusions and Future Work .....	31
	<b>Appendix A: Circle and Semicircle Comparison Plots</b> .....	<b>32</b>
	<b>Bibliography</b> .....	<b>35</b>
	<b>Index</b> .....	<b>36</b>

# List of Figures

---

<b>Figure 1.1</b> Map of the International Monitoring System infrasound network..	10
<b>Figure 1.2</b> Measurements from both seismic and infrasound sensors at the same time and same location over two days.	11
<b>Figure 2.1</b> Setup of explosives at workshop in Buffalo.	16
<b>Figure 2.2</b> Volcano Hazards Workshop Setup	17
<b>Figure 2.3</b> Image showing balloons being filled	18
<b>Figure 2.4</b> Shape of each respective crater. The blue balls represent the balloons.	19
<b>Figure 2.5</b> Photograph images of each crater with the balloons placed inside.	19
<b>Figure 2.6</b> Diagram of setup.	20
<b>Figure 2.7</b> Geometric depiction of how microphone locations on circles ( $r = 20$ m) concentric with the four craters (pads) are projected to semicircle of $r = 38$ m centered on $(0,0)$ .	21
<b>Figure 2.8</b> Weak-shock propagation vs. spherical spreading	23
<b>Figure 2.9</b> Attenuation due to different effective flow resistivities.	25
<b>Figure 3.1</b> Polar Plots of SEL for the four craters originally Figure 4 in Escobedo 2018.	27
<b>Figure 3.2</b> Pressure waveform at 90 degrees on circle centered on crater 1 with microphone height of 4 ft.	28
<b>Figure 3.3</b> Pressure peak comparison of spherically propagated circle data to semicircle data for crater 1 at microphone heights of 4 ft (first test)	30

# List of Tables

---

**Table 2.1** Effective flow resistivities for different surfaces. .... 24

# Chapter 1 Introduction

---

## 1.1 Motivation

Volcano detection is important for many reasons. One being that volcanic eruptions eject ash into the atmosphere and can cause damage to planes flying overhead. A notable volcano, the Icelandic Eyjafjallajökull volcano, erupted in 2010, completely shutting down air travel across Europe for a week [Perkins 2011]. Because of the remote location of many volcanoes many are observed via satellites. However, satellites can be blocked by cloud coverage etc. Thus, multiple methods of detection are necessary. In addition to satellites, seismic sensors (ground vibration sensors) and infrasound sensors (below audible frequencies sensors) are used to detect volcanoes. This research relates to detection via infrasound and using infrasound to better understand the directionality of the ejected ash content.

## 1.2 Background

### 1.2.1 Volcano Acoustics

One main goal of Volcano Acoustics, which has already been mentioned, is to detect volcanic eruptions. Infrasound sensors are already in place worldwide, as seen in Figure 1.1, and used primarily to enforce the nuclear test ban treaty. These infrasound sensors are also used, in conjunction with satellite and seismic data, to detect volcanic activity.

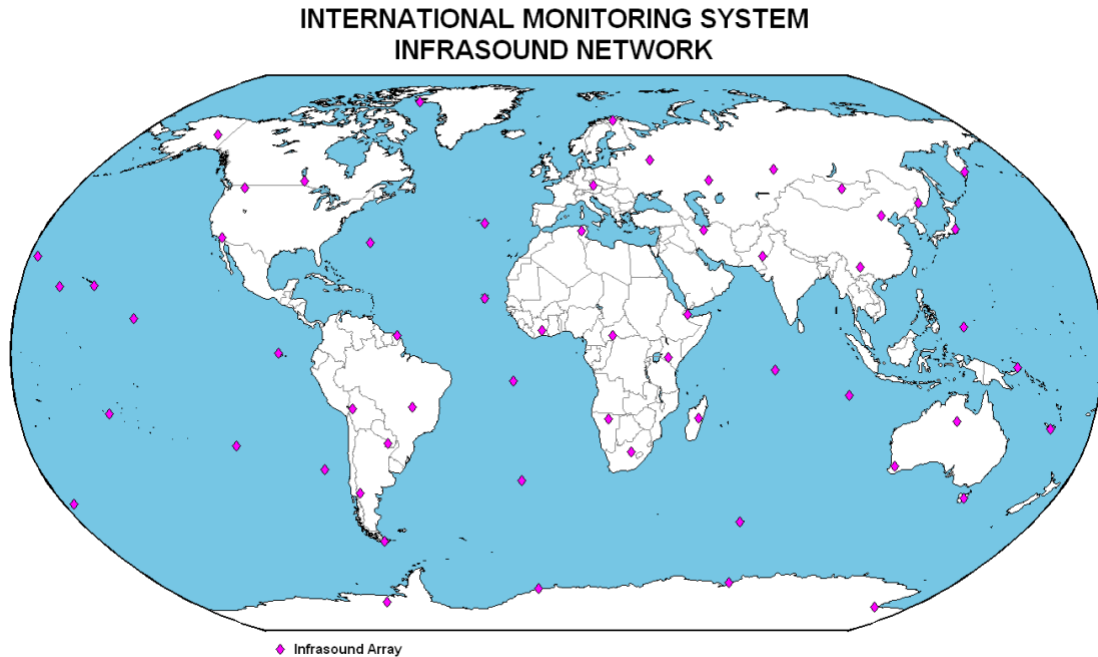


**Figure 1.1** Map of the International Monitoring System infrasound network. Purple diamonds mark infrasound sensor locations. [From Matoza *et al.* 2017].

While both infrasound and seismic sensors are used to detect volcanoes, infrasound is preferable in most cases because it is easier to recognize volcanic eruptions in infrasound data than in seismic measurements. For example, Figure 1.2 shows two sets of data collected at the same location over the same two days. One volcanic eruption occurred, but there were other sources of seismic activity; thus, determining the exact time of the eruption is more difficult from the seismic data. However, the eruption is clearly identified in the infrasound data as there were no other prominent infrasound sources.

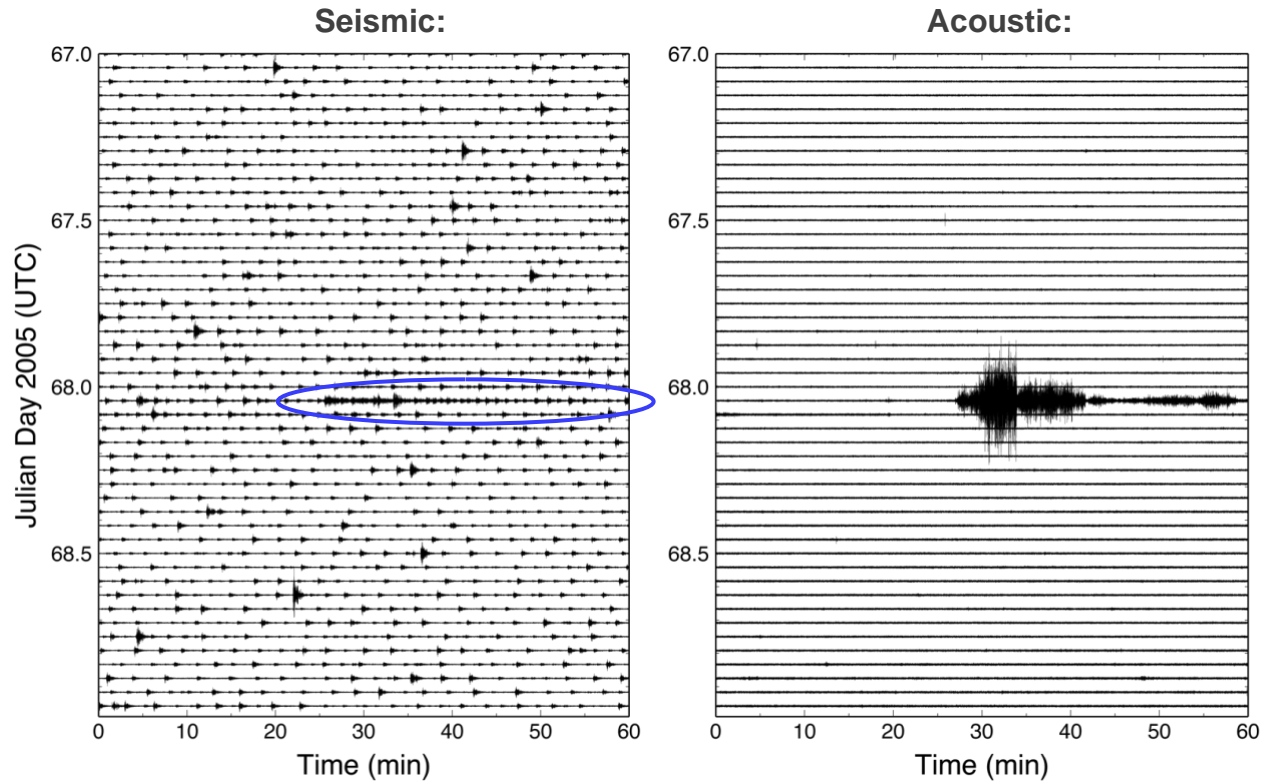


**Figure 1.2** Measurements from both seismic and infrasound sensors at the same time and same location over two days. Each line is an hour over the two days. The blue circled area on the seismic chart is when the volcano erupted. The acoustic data is much clearer. [From Matoza 2007]

The primary goal of my research is estimating the directionality of volcanic ash content from the directionality of propagated sound. This research focuses on the directionality of the propagated sound from scale-model volcanoes. Further research is needed to show how the propagated sound relates to directionality of ash. The shape of the crater might influence directionality of both sound and ash content [Bowman 2014]. This research is one step in order to better understand these relationships.

## 1.2.2 Explosions as Scale-Model Volcanoes

To help understand volcanic behavior, controlled explosions were used as scale-model volcanoes in this research. Explosions create impulsive sound waves like are present in explosive

volcanic activity. While man-made explosions differ from volcanoes, many of the insights learned from explosions can be applied to volcanoes.

Explosions are easier to study than volcanoes. Experiments with explosions are controllable since they can be set up rather than just observed. Explosions are smaller scale and can be tested at many open locations, while volcanoes can only be studied at their respective locations. Explosion craters can be pre-shaped or can be viewed easier and closer afterward. Explosions are also more repeatable than volcanic eruptions. A more controlled experiment is possible with explosions rather than volcanoes.

The differences between the sound from explosions and volcanoes are also important to note. The explosions are smaller than volcanic eruptions so higher frequencies are more prevalent. The primary frequencies of volcanoes are less than 20 Hz (Hertz) [Matoza *et al.* 2019]. The frequencies of explosions tested in this study is 100 Hz and less. Consequently, the time scale associated with explosions is shorter and requires a higher sampling rate than volcano studies.

In 2018, we worked with Robin Matoza from the University of California, Santa Barbara (UCSB) on two experiments. The main experiment was at a volcano hazards workshop at the University of Buffalo with a series of buried pentaerythritol tetranitrate (similar to C-4) explosions. To prepare for this large experiment, our BYU acoustics group conducted a pretest using exploding oxy-acetylene balloons.

### **1.3 Prior Work**

Previous work studying volcanoes was done by Robin Matoza, a collaborator from the University of Santa Barbara. His studies of volcanoes led to this work. His papers include many

clear introductions into studying volcanoes as well as studies of specific volcanoes [Matoza 2017 and 2018a]. These studies address the use of the international monitoring station to detect infrasound activity.

Studies using buried explosions and analyzing crater shape have also been done [Ohba 2002]. Ohba *et al.* used dynamite to explore the energy, depth and nature of the explosion cloud due to crater depth. They showed that for shallow depths, scaled height and scaled duration of the cloud increased as scaled depths increased. How the explosion cloud changes due to crater depth is applicable to the workshop test since multiple depth were used.

Previous workshops similar to the one we participated in have been conducted at the University of Buffalo Geohazards Field Station [Ball 2011]. These workshops also used explosions to model volcanic activity.

To prepare for the workshop with buried explosives, our group conducted a pretest using exploding balloons. These oxy-acetylene balloons were used as an impulsive source in a previous set of studies at BYU [Young 2015]. Sarah Young *et al.* compared peak levels of exploding oxy-acetylene balloons with predictions from weak-shock theory and found good agreement out to 1 mile. Spherically decaying shocks were also discussed. Young *et al.* concluded shock wave behavior is evident closer to the source than previously stated in other sources. A study by Leete *et al* examines how reflected waves travel quicker than the shock wave and form Mach stems [Leete 2015]. Both these studies used balloons placed above the ground, whereas in our pretest, the balloons are on/in the ground.

This research focuses on the directionality of sound from explosion tests. However, data used to determine the seismic-acoustic wave coupling was also collected. Further analysis is still needed to make conclusions using that data. Although not addressed in this paper, some of the

preliminary work is recorded in more depth elsewhere in References [Lysenko 2019] and [Escobedo 2018].

## **1.4 Overview**

The goal of my research is to estimate the acoustic directionality of explosions using a non-concentric semicircle microphone array for the volcano hazards workshop. We measured buried explosives at four test sites using an array of microphones in a semicircle. The sites were relatively close together, but our array was centered on none of them. Instead we centered it between all four sites. In order to interpret our data, we performed a pretest using exploding balloons. In this test, we took measurements using a single non-concentric arc and circular arcs centered on each balloon location. This study strives to connect the concentric directionality to the non-concentric directionality. Spherical spreading accounts for most of the difference, but the propagation of sound over the porous ground must also be considered. Chapter 2 describes the methods and experimental setups. Chapter 3 discusses our results, conclusions and future work. This thesis outlines the theory, experimental setup and analysis of the acoustic directionality of explosions as scale-model volcanoes.

# Chapter 2    Methods

---

The goal of this research is to estimate the directionality of explosions from measurements on an arc not concentric with the origin of the explosion. This chapter outlines the setups used in the two tests conducted—one using buried explosives and the other using oxy-acetylene balloons. In order to analyze the data collected, certain principles—nonlinear propagation, spherical spreading and effective flow resistivity—need to be understood and are thus introduced in this chapter.

## 2.1 Buried Explosives Test

### 2.1.1 Summary

Measurements of buried explosives were taken at a workshop in Buffalo, New York on July 26, 2018. This workshop was called the Multidisciplinary Volcano Hazards Experiments at the Geohazards Field Station [Valentine 2018]. At the workshop, we measured the pressure levels of propagated sound from buried explosives similar to C-4. Explosives were buried at four test sites, or pads. These pads were in a horizontal row separated by 4-5 m. At each test site, six explosives were buried in the different configurations shown in Figure 2.1. For each site, the charges detonated at intervals of 0.5 sec, beginning with the upper ones.

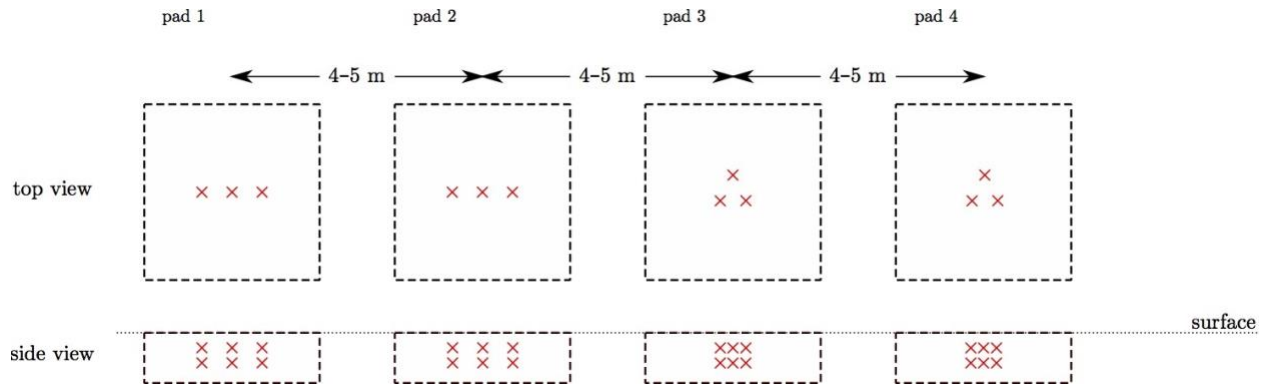


**Figure 2.1** Setup of explosives at workshop in Buffalo. Each 'x' marks an explosive location. Both top view and side view are shown for each pad.

### 2.1.2 Semicircle Microphone Array

We measured the explosions using different configurations of microphones attached to dowels on tripods arranged as shown in Figure 2.2. The red circles in the center represent the four explosion sites. Around these test sites, we set up a semicircle array of microphones, represented by the green circles, to measure the directionality of the propagated sound and how it relates to crater shape. We had microphones at heights of 4 ft and 8 ft from 0 degrees to 180 degrees with 30-degree spans. This array was centered on the middle of all of the test sites. We were unable to center our semicircle array on any individual pad since we could not move the microphones during tests. Thus, this array was not concentric with any of the blast locations, which complicates estimates of directionality.



**Figure 2.2** Volcano Hazards Workshop Setup. Image of the four explosion test sites represented by the small red circles. The small green circles represent the microphone locations arranged in a semicircle around the center of the test sites.

## 2.2 Oxy-Acetylene Balloons Test

### 2.2.1 Summary

Since a nonconcentric semicircle arc was used in the Buffalo test, we needed to learn how to connect directionality on a nonconcentric arc to that from a concentric arc. Thus, we performed a test with both concentric arcs for each blast location as well as a nonconcentric arc. This pretest was conducted in a farmer's empty field in Provo, Utah on July 11, 2018. Taller grass and weeds were cleared.

We used oxy-acetylene filled balloons as explosions. The gas mixture satisfies the chemical equation  $2C_2H_2(g) + 5O_2(g) \rightarrow 4CO_2(g) + 2H_2O(g)$  [Escobedo 2018]. Rings of polyethylene tubing were used to fill the balloon with the necessary volumes of each gas as seen in Figure 2.3. Each researcher completed training in order to properly handle the tanks containing the various gasses.



**Figure 2.3** Image showing balloons being filled. The different rings were used to fill the balloon with the proper volumes of each gas.

The balloons, each with a diameter of 43.18 cm, were placed in four specially designed craters, as illustrated in Figure 2.4. Photographs shown in Figure 2.5. The craters were dug in the ground, and the balloons were placed in or on the craters. Crater 1 consisted of the balloon simply placed in a small divot in the ground. This crater was designed as a control reading of the acoustic shock for a source on the ground. Crater 2 involved a balloon placed in a hole with 3 ridges dug into a single side of the hole. This design was based on directional fracturing of rock [Isakov 1983]. Crater 3 was a set of two balloons, one the same size as the others used in the previous craters and the other balloon of 35.56 cm diameter. The regular sized balloon was set in a hole with the smaller balloon set in an offshoot in the bottom of the hole. This design was based off of a land mine detonator [Reuther 1963]. The smaller balloon would be ignited by the larger balloon and the two shock waves would combine. Crater 4 consisted of a balloon placed in a cylindrical hole. This last crater allowed us to compare below-ground and on-the-ground measurements.

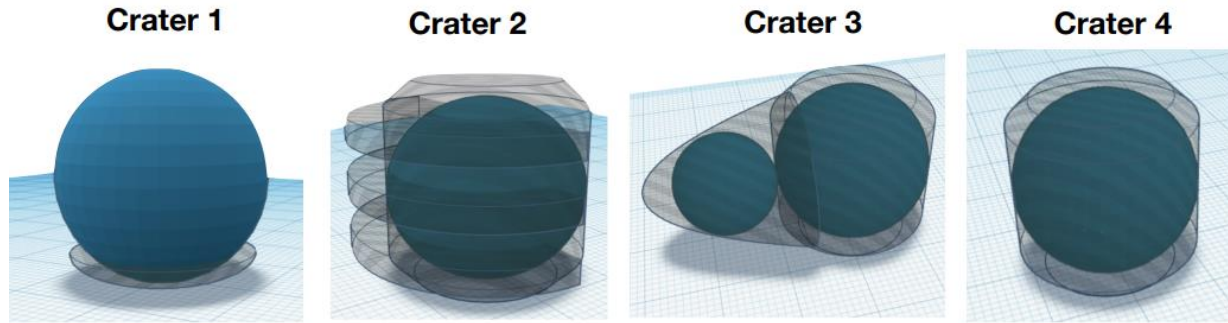


**Figure 2.4** Shape of each respective crater. The blue balls represent the balloons. The translucent gray objects represent the shape of the holes dug for each balloon. [Figure 3 from Escobedo 2018].



**Figure 2.5** Photograph images of each crater with the balloons placed inside. The saran wrap was used to prevent the balloons from popping prematurely.

### 2.2.2 Circular Microphone Arrays

Similar to the experiment in Buffalo, we also used circular microphone arrays to determine the directionality of the sound. Microphones were placed at heights of 4 ft and 8 ft. We used two different configurations as shown in Figure 2.6. One set of tests was conducted using a semicircle microphone array, from 0 degrees to 180 degrees every 30 degrees, at 38 m out from the center of all the craters. This array is represented in Figure 2.6 by the green dots along the outer red circle. The semicircle array was not concentric to any one crater location, similar to the Buffalo test. A second set of tests was conducted using circular arrays, 0 degrees to 330 degrees every 30 degrees, at 20 m from the center of each individual crater location. These arrays are represented in the figure by the green dots along the yellow circles. The four circular

arrays were concentric with each of the four crater locations. For all arrays, 0 degrees was to the south and 180 degrees was to the north, as labeled in Figure 2.6. The circle and semicircle arrays from this pretest were used to better understand the non-concentric semicircle used for the Buffalo workshop.

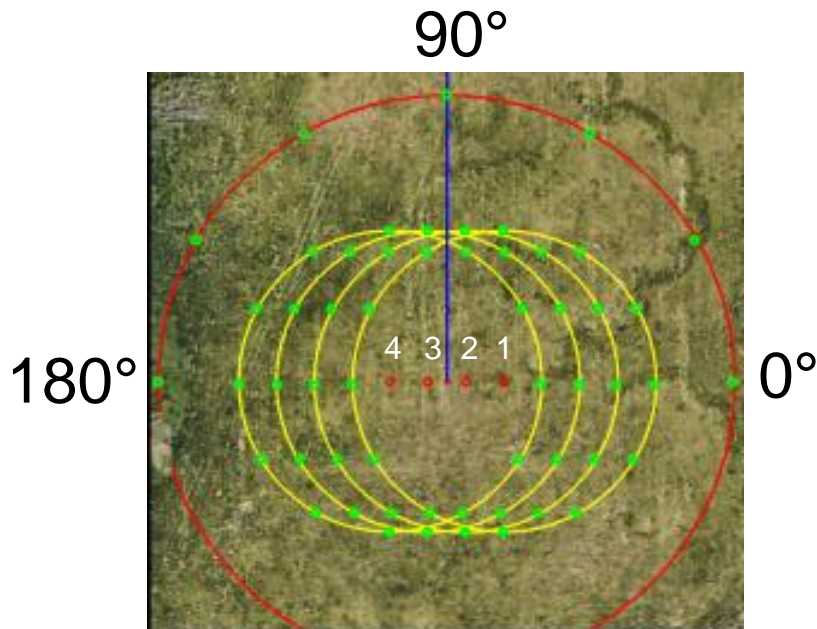


**Figure 2.6** Diagram of setup. The craters are labeled in the center (1-4) corresponding to each respective shape as previously defined. The southside of each array is labelled as 0° and the north as 180°. The green dots on the red circle represent the semicircle microphone array locations while the green dots on the yellow circles represent the circle microphone array locations.

## 2.3 Spherical vs. Nonlinear Propagation

Spherical spreading methods are used to compare the circle data (at  $r = 20$  m) to the semicircle data (at  $r = 38$  m). As stated previously, the circle arrays were centered on individual blast locations, however the semicircle was non-concentric as shown in Figure 2.7. The change in sound levels measured at distance  $r_1$  due to spherical spreading to a distance  $r$  is computed by adjusting the peak level to account for difference in distance:  $20 \log_{10} r_1/r_2$ . The data of the circle arrays (at 20 m from the center of each circle) were scaled to 38 m from the center of the

semicircle in order to compare with the data from the semicircle array. Thus,  $r_1$  is the distance from the center of the semicircle to a point on the circle, and  $r_2$  is the distance from the center of the semicircle to the projected point on the semicircle as shown in Figure 2.7. Each crater location is marked by boxes and the locations of the microphones centered around each crater are marked by small circles. Only half of each circle is shown in order to compare to the semicircle array. In the figure, the stars represent the propagated locations of the circle data onto the semicircle of radius 38 m. Lines connect the circles to the stars to show the distances  $|r_2 - r_1|$  each data point was propagated in order to match with the semicircle. For example, the black circle at 30 degrees—on the right, second to bottom—follows the black line out to the black star showing the new (propagated) location in reference to the semicircle. As seen in the figure, not all the distances between circles and stars,  $|r_2 - r_1|$ , are the same for each point on each circle because the distance from the center of each respective circle was a different distance away from the center of the semicircle. These distances were used to compute the spherically spreading prediction for peak level.

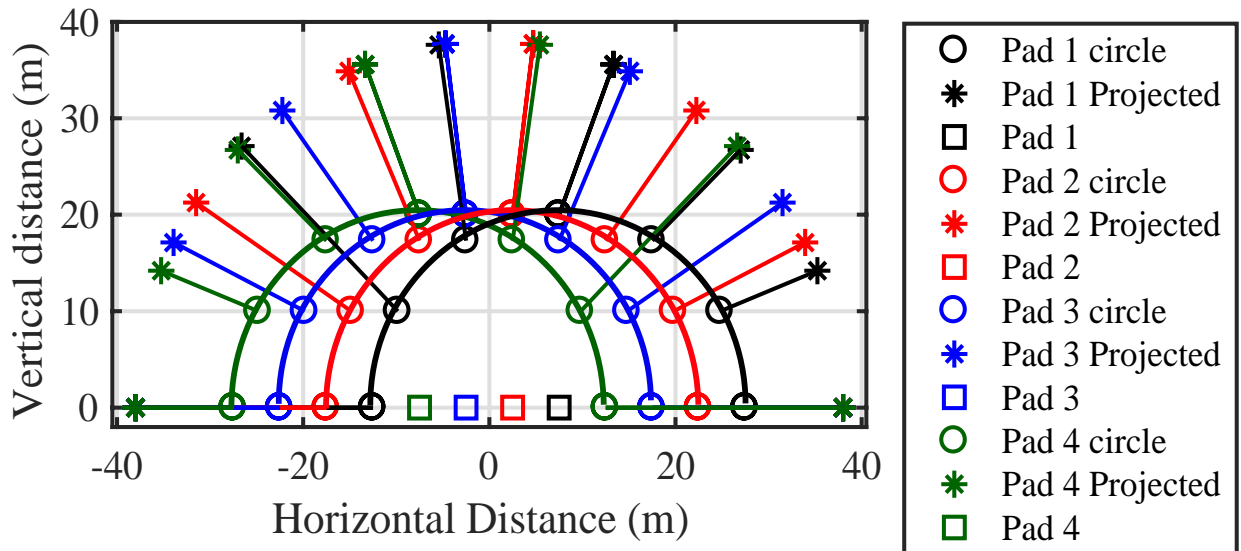


**Figure 2.7** Geometric depiction of how microphone locations on circles ( $r = 20$  m) concentric with the four craters (pads) are projected to semicircle of  $r = 38$  m centered on  $(0,0)$ .

Since the explosions produce shock waves, the potential for non-linear propagation needed to be accounted for. Nonlinear propagation occurs when the amplitude is loud enough that the linear approximation is not sufficient, meaning the behavior of the propagation does not agree with the common spherical spreading [Leete 2015]. To determine the uncertainty in predicted levels due to nonlinear propagation, comparisons were made between a linear (spherical) and nonlinear (weak shock theory) propagation. Figure 2.8 is from a previous test by Young *et al.* using oxy-acetylene balloons. The horizontal axis shows distance, on a log scale, and the vertical axis shows the peak sound pressure level ( $L_{pk}$  in dB). The red dots represent the data points, and the black lines are two weak-shock fits representing nonlinear propagation. The cyan line was added for the current work to show the estimated change in level due to linear propagation (spherical spreading) beginning near 12 m, which is the smallest  $r_1$  in Figure 2.7. As seen in Figure 2.8 Weak-shock propagation vs. spherical spreading. The original version is Figure 4 in Young *et al.* 2015. The red dots show the data used with permission from Young *et al.* The black lines show two different fits using weak-shock theory. The cyan line has been added to show the spherical spreading approximation in the range of interest., between distances of 12 m and 38 m (where the nonconcentric semicircle array is located), only about 1 dB error exists between the change in level from spherical spreading and nonlinear propagation. Thus, the error associated with not using non-linear shock propagation when propagating circle array data to semicircle distances is approximately 1 dB. Thus, in Chapter 3, spherical spreading is used to model the propagation of sound between the circle and semicircle arcs.

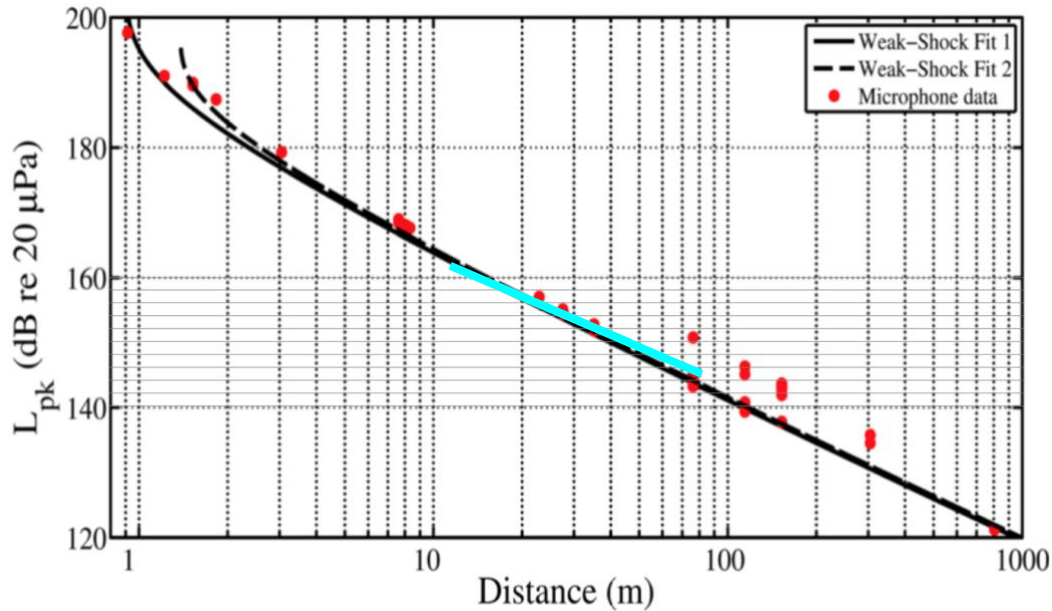


**Figure 2.8** Weak-shock propagation vs. spherical spreading. The original version is Figure 4 in Young *et al.* 2015. The red dots show the data used with permission from Young *et al.* The black lines show two different fits using weak-shock theory. The cyan line has been added to show the spherical spreading approximation in the range of interest.

## 2.4 Effective Flow Resistivity

These spherical spreading propagations are complicated by the interaction of the sound with the porous ground. To investigate this effect, the effective flow resistivity is modeled. The effective flow resistivity (EFR) is a measure of how much sound attenuates due to different ground types. In Table 2.1, many types of surfaces as well as their respective EFRs in cgs rayls—are referred to simply as rayls in this paper—are displayed [Embleton 1983]. EFR measures are used to predict the impact of ground reflection on the frequency spectra of sound. Since our exploding balloon test was measured on a grass-covered field, this EFR  $\sim 150$ -300 rayls is important to take into account when analyzing our data. This analysis has yet to be conducted, but we will analyze our data in the frequency domain in the future to determine if the EFR varied around the circle.

**Table 2.1** Effective flow resistivities for different surfaces. Data taken from Embleton 1983.

<b>Surface Type</b>	<b>Snow</b>	<b>Forest Floor</b>	<b>Grass</b>	<b>Loose Dirt</b>	<b>Packed Dirt Roadway</b>	<b>Rain-Packed Dirt</b>	<b>Asphalt</b>
<b>Flow resistivity (cgs rayls)</b>	<b>10-50</b>	<b>20-80</b>	<b>150-300</b>	<b>300-800</b>	<b>2000-4000</b>	<b>4000-8000</b>	<b>30000</b>

Variations in the spectra for different EFRs can be seen in Figure 2.9. The horizontal axis shows the frequencies (in kHz), and the vertical axis shows the relative SPL (in dB). The different curves correspond to different values of EFR with the respective  $\sigma$  values listed beside each one. Certain types of ground tend to attenuate sound more at certain frequencies for a specified source-receiver configuration. In the example in Figure 2.9, grass has an EFR of 150-300 rayls which tends to attenuate—decrease the sound level of—frequencies around 1 kHz and 6 kHz. Whereas, asphalt closely follows the  $\sigma = 32\ 000$  curve showing a large attenuation at around 3 kHz. Further analysis of our data in the frequency domain will help us determine if the EFR varied at different degrees around the circles.

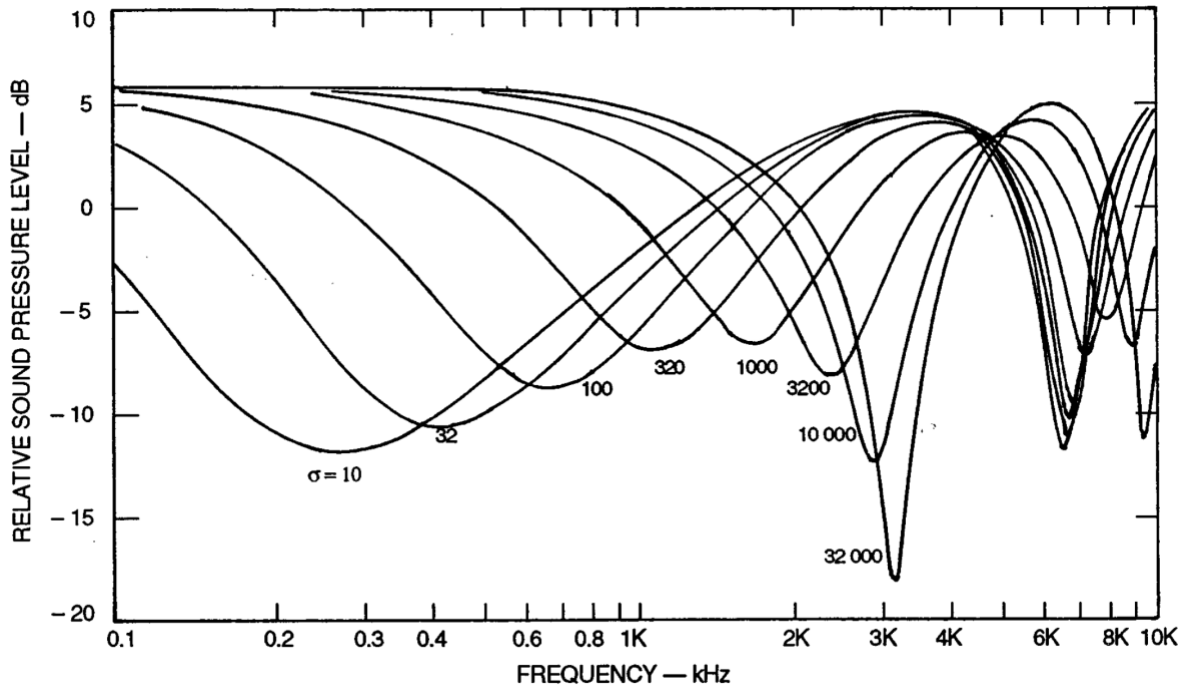


**Figure 2.9** Attenuation due to different effective flow resistivities. Curves are calculated for source and receiver heights, and their separation of 0.31, 1.22, and 15.2 m respectively. The effective flow resistivity  $\sigma$  varies from 10 kPa·s/m<sup>2</sup>, by a factor of 3.2 for successive curves, to 32 000 kPa·s/m<sup>2</sup> [Borrowed from Embleton 1983].

# Chapter 3 Analysis and Results

---

## 3.1 Oxy-Acetylene Balloons Analysis

The goal of this research is to estimate the directionality of explosions from measurements on an arc not concentric with the origin of the explosion. This chapter outlines the analysis done for the two tests conducted—one using buried explosives and the other using oxy-acetylene balloons. Nothing conclusive has been found so far, but preliminary results are shown.

### 3.1.1 Preliminary Directionality Analysis

For the oxy-acetylene balloon test, the sound exposure levels (SEL)—overall levels for the entire waveforms—from the circle data were used to initially analyze the directionality of each crater. Preliminary directionality plots were made by Julio Escobedo shown in Figure 3.1 [Escobedo 2018]. The four plots show the directionality of the four craters, with the title of each referring to each respective crater. Each individual plot shows 0-330° labeled around the outside circle of the plot. The data from the 4 ft first and second test are shown with the red and blue lines respectively. The data from the 8 ft first and second test are shown with the yellow and purple circles respectively. The labels on each of the inner circles as well as the label on the outer circle refer to the SEL. Crater 1 appears to be the most omni-directional—SEL within 0.5 dB—which was expected since this was the balloon placed in a small divot in the ground. The

other craters show greater than 1 dB variation in SEL around the circle that differs for each crater. For the remainder of this work, the peak levels of the blast are used to better understand the directionality of the other craters.

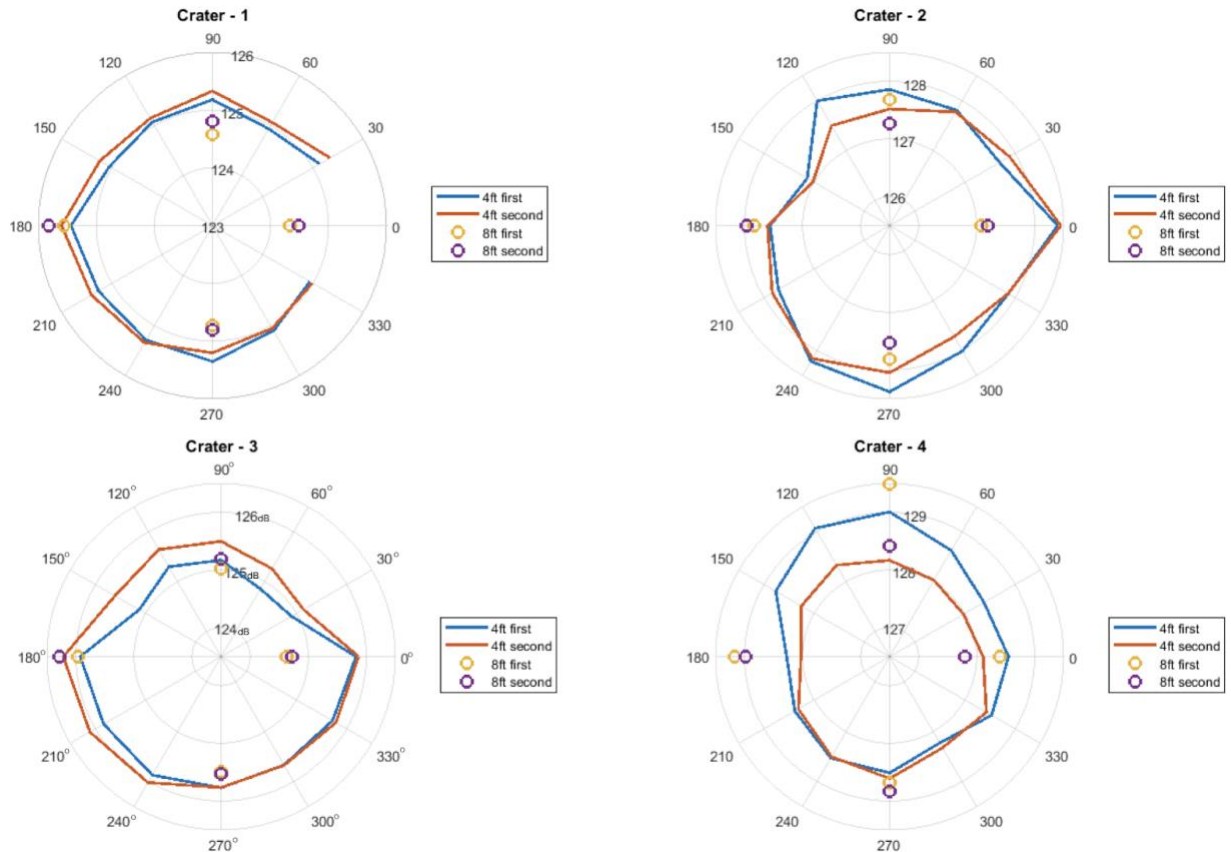


**Figure 3.1** Polar Plots of SEL for the four craters originally Figure 4 in Escobedo 2018. The blue and red lines represent the SEL from the 4 ft first and second test respectively, and the yellow and purple small circles represent the SEL from the 8 ft first and second test respectively. [Escobedo 2018].

### 3.1.2 Identifying Peaks in Waveforms

Since the value needed for determining the directionality of the shock wave is the peak pressure, the next step to processing our data was to look at the waveforms and determine the peak levels. The blast peak is the first large pressure value after the rapid rise—when the waveform looks nearly vertical. For microphones at heights of 8 ft above the ground, this first

peak is also the peak of the waveform. However, for microphones at 4 ft, the peak of the entire waveform happens after the blast peak as seen in Figure 3.2. This figure shows the time-varying pressure waveform measured at 90 degrees on the circle centered on crater 1 at a height of 4 ft. The peak of the overall waveform, marked by the blue 'x,' is the secondary arrival, the ground wave. This peak is larger than the blast peak, marked by the red 'o,' so simply using the maximum values of each waveform leads to incorrect directivity for the blast wave. Thus, the peaks of the blast needed to be determined.

When finding the blast peaks, Gibb's phenomenon had to be taken into account. Gibb's Theorem states that a shockwave results in a 9% overshoot when recording data [Smith 2003]. Thus, the actual peak pressure (red circle in Figure 3.2) is 9% less than the peak value that was recorded.

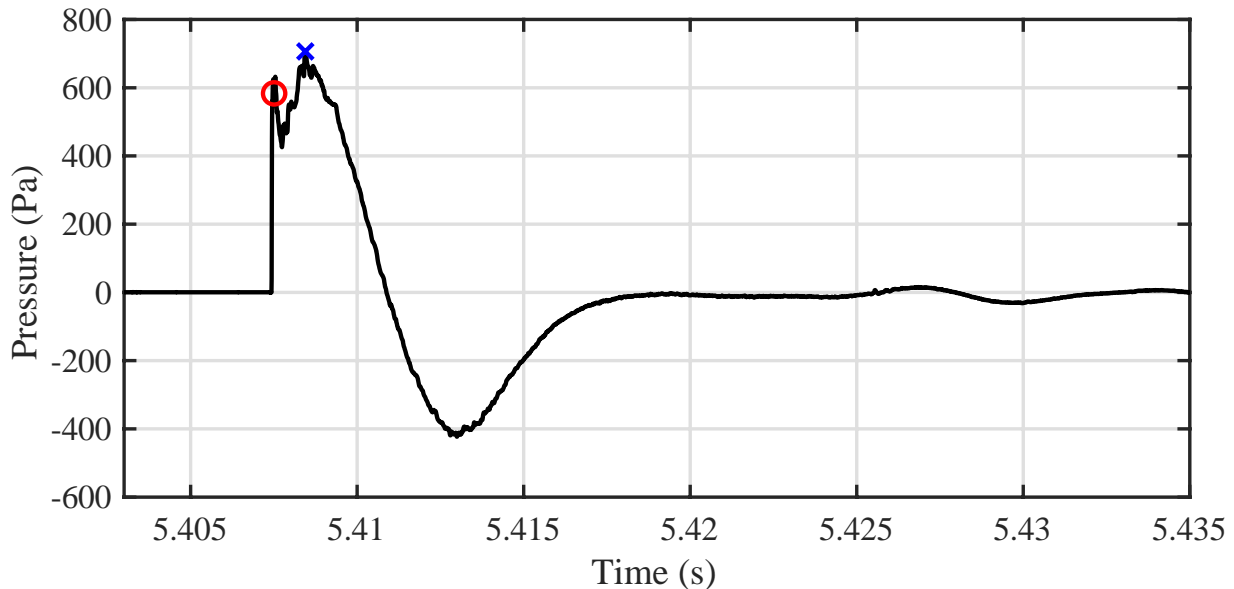


**Figure 3.2** Pressure waveform at 90 degrees on circle centered on crater 1 with microphone height of 4 ft. The red 'o' denotes the blast peak while the blue 'x' denotes the ground peak. Note the red 'o' shows the true peak which is 9% lower than the measured value due to Gibb's theorem [Smith 2003].

### 3.1.3 Circle and Semicircle Comparisons

Since we could only measure the workshop explosions using a nonconcentric semicircle arc, we needed a way to compare concentric circle data and nonconcentric semicircle data. Thus, both types of circular arrays were used during the balloon test. Determining how to compare the circle peak values with the semicircle peak values required a method to propagate the circle data out to the distances of the semicircle data. Spherical spreading was used to project the circle data onto the semicircle shown in Figure 2.7. As shown in Section 2.3, the neglect of nonlinear propagation over these distances leads to an estimated error of 1 dB.

Comparisons between the spherically propagated circle blast peak levels,  $L_{\text{blast}}$ , and the semicircle  $L_{\text{blast}}$  are shown in Figure 3.3. This graph shows levels from crater 1 at microphone height of 4 ft for the first test. Similar plots for other craters, heights and tests are found in Appendix A; the general shapes are the same as the case in Figure 3.3. The horizontal axis shows the degrees around the semicircle. The vertical axis shows the  $L_{\text{blast}}$  values (in dB). The circle levels are represented by the circles, the spherically propagated circle levels are represented by the stars, and the semicircle levels are represented by the diamonds. The goal is to determine how close the stars are to the diamonds—or how close the spherical propagation approximation is to the actual data from the semicircle.

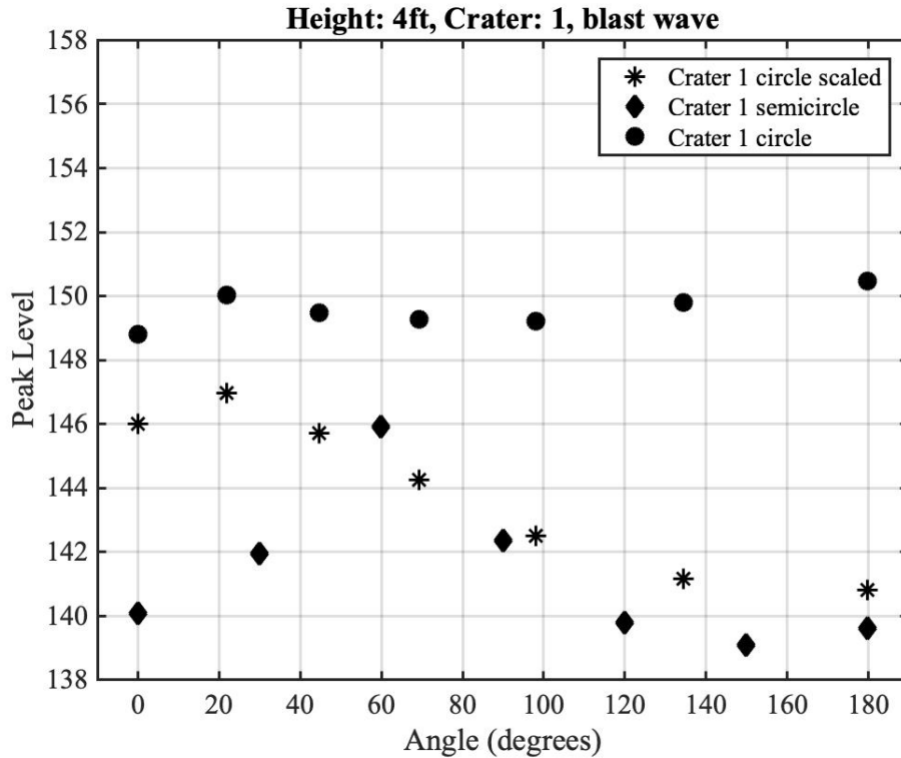


**Figure 3.3** Pressure peak comparison of spherically propagated circle data to semicircle data for crater 1 at microphone heights of 4 ft (first test). The horizontal axis shows the angle around the semicircle and the vertical axis shows the blast peak level (in dB). The circles represent levels at the 20 m circle concentric with crater 1, the stars the propagated circle levels to the 38 m semicircle and the diamonds the measured semicircle levels. For similar plots for other craters and/or heights see Appendix A.

At some angles, the propagated circle levels are close in value with the semicircle data. Specifically, the projected levels (\*) are within 2 dB for 60°–180°. However, at smaller angles unexpected discrepancies exist. The projected levels are 4-6 dB higher than the semicircle array levels at 0° and 30°. This spatial variation exists for other craters as well, which implies that something was different about the propagation in the 0°–30° direction than at other angles.

In the future, we need to determine the reasons behind the spatial variation. One way in which these data points differ may be due to the effective flow resistivity of the ground (as explained in Section 2.4) and how it varies around the circle. Further analysis of our data in the

frequency domain will help us determine if the EFR varied at different degrees around the circles. Another possible explanation for this discrepancy is due to astrological changes between when the data was collected for the circles versus the semicircle.

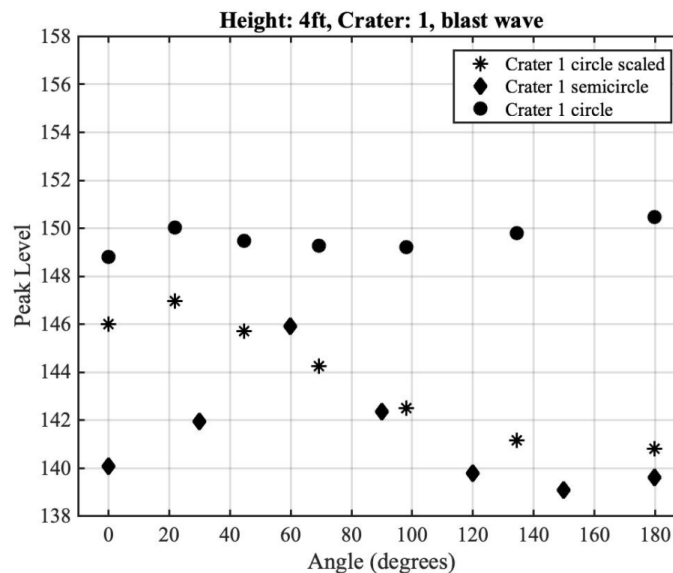
## **3.2 Conclusions and Future Work**

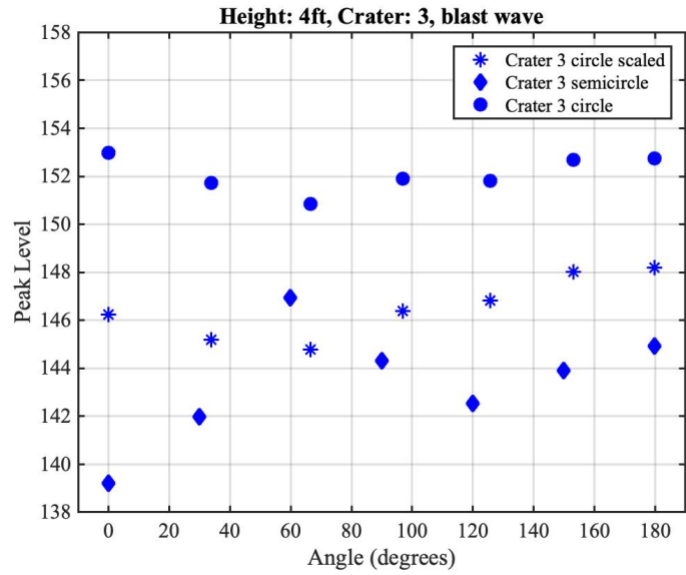
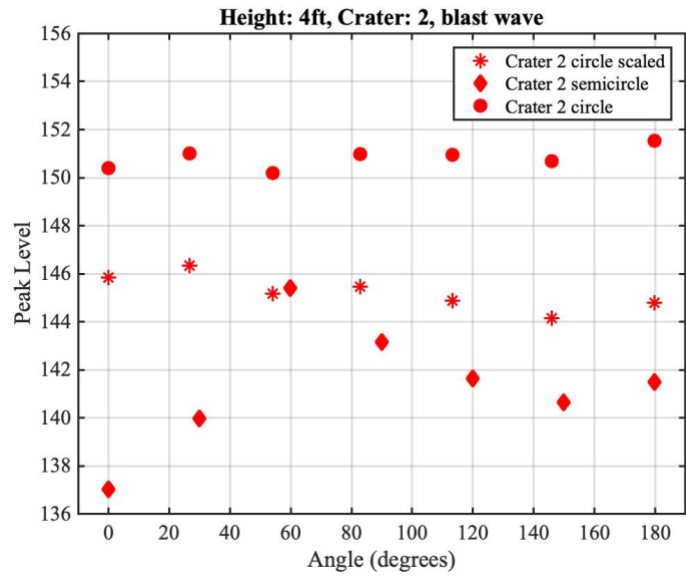
In conclusion, spherical spreading is a good approximation for the shock waves studied in this work. Since the workshop test was also over porous ground, determining the reason for the spatial variations in the pretest, will lead to an even better understanding of the directionality in the workshop test. We plan to use future conclusions from the pretest about non-concentric semicircle arrays in order to determine the directionalities of the explosions in the workshop test.

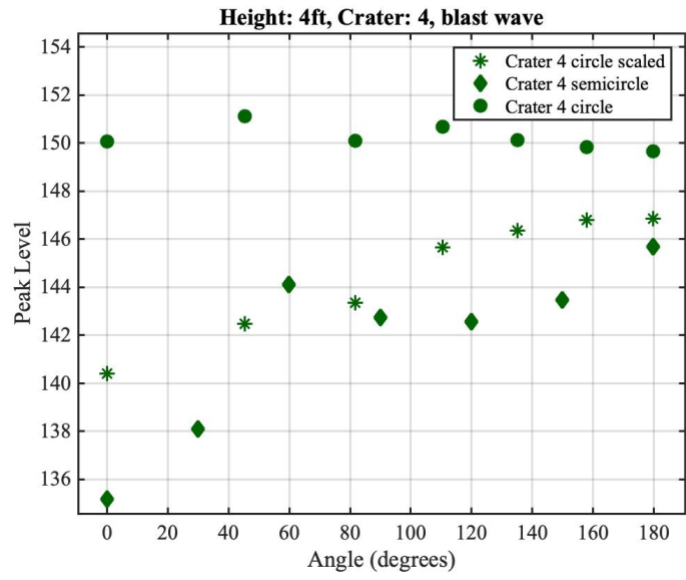
# Appendix A: Circle and Semicircle Comparison Plots

---

The following plots show peak blast levels for the balloon test, similar to Figure 3.3. The first plot shows the comparison between the propagated circle peak values and semicircle peak values for crater 1 for microphones at 4 ft. The next plot shows similar data for crater 2 at 4 ft. The third plot shows the comparison for crater 3 and the fourth plot shows the data for crater 4. Similar comparisons were done for microphones at 8 ft. These plots were created using the peak value from the blast in each waveform. Comparisons were also made using the peaks from the peak of the ground wave in each waveform.







# Bibliography

- Ball, Jessica. "Buffalo Gets Some (Experimental) Volcanic Action." AGU, 5 Apr. 2011, [blogs.agu.org/magmacumlaude/2011/03/31/buffalo-gets-some-experimental-volcanic-action/](https://blogs.agu.org/magmacumlaude/2011/03/31/buffalo-gets-some-experimental-volcanic-action/).
- Bass, H. E., Bolen, L. N., Cress, D., Lundien, J., & Flohr, M. (1980). Coupling of airborne sound into the earth: Frequency dependence. *The Journal of the Acoustical Society of America*, 67(5), 1502-1506.
- Bowman, D. C., Taddeucci, J., Kim, K., Anderson, J. F., Lees, J. M., Graettinger, A. H., ... & Valentine, G. A. (2014). The acoustic signatures of ground acceleration, gas expansion, and spall fallback in experimental volcanic explosions. *Geophysical Research Letters*, 41(6), 1916-1922.
- Escobedo, J. "Measuring Directionality of Acoustic Shocks from Small Scale Explosions." Project for Master's of Secondary Science Teaching, University of Utah, Dec. 2018.
- Isakov, A.L. Directed fracture of rocks by blasting. *Soviet Mining Science* 19, 479–488 (1983). <https://doi.org/10.1007/BF02497175>
- Leete, K. M., Gee, K. L., Neilsen, T. B., & Truscott, T. T. (2015). Mach stem formation in outdoor measurements of acoustic shocks. *The Journal of the Acoustical Society of America*, 138(6), EL522-EL527.
- Lysenko, E. "Direct Measurement of Seismo-acoustic Wave Coupling." BYU Department of Physics and Astronomy Senior Thesis Report. 2019. <https://www.physics.byu.edu/library/theses>.
- Matoza, R. S., Green, D. N., Pichon, A. Le, Shearer, P. M., Fee, D., Mialle, P., and Ceranna, L. (2017), Automated detection and cataloging of global explosive volcanism using the International Monitoring System infrasound network, *J. Geophys. Res. Solid Earth*, 122, 2946–2971, doi:10.1002/2016JB013356.
- Matoza, R. S., Fee, D., Green D. N., Mialle P. (2019), Volcano Infrasound and the International Monitoring System. In: Le Pichon A., Blanc E., Hauchecorne A. (eds) *Infrasound Monitoring for Atmospheric Studies*. Springer, Cham
- Matoza, R. S., & Fee, D. (2018a). The inaudible rumble of volcanic eruptions. *Acoustics Today*. 14(2), 17-25.
- Ohba, T., Taniguchi, H., Oshima, H., Yoshida, M., & Goto, A. (2002). Effect of explosion energy and depth on the nature of explosion cloud: A field experimental study. *Journal of Volcanology and Geothermal Research*, 115(1-2), 33-42.
- Perkins, Sid. "2010's Volcano-Induced Air Travel Shutdown Was Justified." *Science Magazine*, 25 Apr. 2011, [www.sciencemag.org/news/2011/04/2010s-volcano-induced-air-travel-shutdown-was-justified#](http://www.sciencemag.org/news/2011/04/2010s-volcano-induced-air-travel-shutdown-was-justified#).
- Reuther, H. G. (1963). US3090306A - Explosive. United States Patent Office.
- Smith, Steven W. "Chapter 11: Fourier Transform Pairs." *Digital Signal Processing a Practical Guide for Engineers and Scientists*. Newnes, 2003.
- Valentine, Greg. "Facilitating Field-Scale Experiments in Volcano Hazards." *Eos*, 4 Dec. 2018, [eos.org/meeting-reports/facilitating-field-scale-experiments-in-volcano-hazards](http://eos.org/meeting-reports/facilitating-field-scale-experiments-in-volcano-hazards).
- Young, S. M., Gee, K. L., Neilsen, T. B., & Leete, K. M. (2015). Outdoor measurements of spherical acoustic shock decay. *The Journal of the Acoustical Society of America*, 138(3), EL305-EL310.

# Index

## A

Acoustic, i, iii  
arc, 17, 20, 24, 33  
ash, iii, 12, 15

## B

balloons, iii, 16, 17, 20, 21, 22, 23  
blast, 19, 24, 30, 31  
Brigham Young University, i

## C

circle, iii, 23, 24, 26, 29, 31, 32, 33  
concentric  
    non-concentric, iii, 17, 18, 19, 20, 22, 23, 24, 29, 34  
crater, iii, 15, 19, 22, 25, 29, 31, 32, 33

## D

directionality, iii, 12, 15, 17, 19, 22, 29, 30, 34  
directivity, 15

## E

effective flow resistivity  
    EFR, 17, 26, 28, 33  
explosions  
    buried explosions, iii, 15, 16, 17, 18, 19, 29, 34  
Explosions, i, iii, 15, 34

## F

frequencies, iii, 15, 27  
frequency, iii, 26, 27

## G

Gibb's Theorem, 31

## I

infrasound, iii, 12, 14, 15

## M

microphones, 17, 19, 25, 30  
Model, i, iii, 15

## P

peak, 25, 30, 31, 32, 33  
Physics, i, iii  
pressure, 18, 24, 25, 30  
pretest, 16, 17, 20, 23, 34

## S

semicircle, iii, 17, 19, 20, 22, 24, 32, 33, 34  
shock, iii, 16, 23, 24, 32  
sound, iii, 14, 15, 18, 19, 22, 24, 25, 26, 27, 29  
sound pressure level  
    SPL, 24, 25  
spherical  
    spherical spreading, iii, 23, 24, 32

## V

Volcanoes, i, iii, 15

## W

waveform, 30, 31